https://doi.org/10.1007/s11467-024-1424-5

RESEARCH ARTICLE

Giant anomalous transverse transport properties of Co-doped two-dimensional Fe_3GaTe_2

Imran Khan, Jisang Hong†

Department of Physics, Pukyong National University, Busan 48513, South Korea

Corresponding author. E-mail: †hongj@pknu.ac.kr

Received February 4, 2024; accepted May 25, 2024

Supporting information

Table S1 The energy difference (in meV/cell) between AA and AB stacking in bilayer $Fe_{3-x}Co_xGaTe_2$ (x = 0.083, 0.167, 0.250, and 0.330) systems. For reference, the energy of the stable AB stacking is set to zero.

Systems	x=0.083	x=0.167	x=0.25	x=0.33
AB	0	0	0	0
AA	523	539	555	544

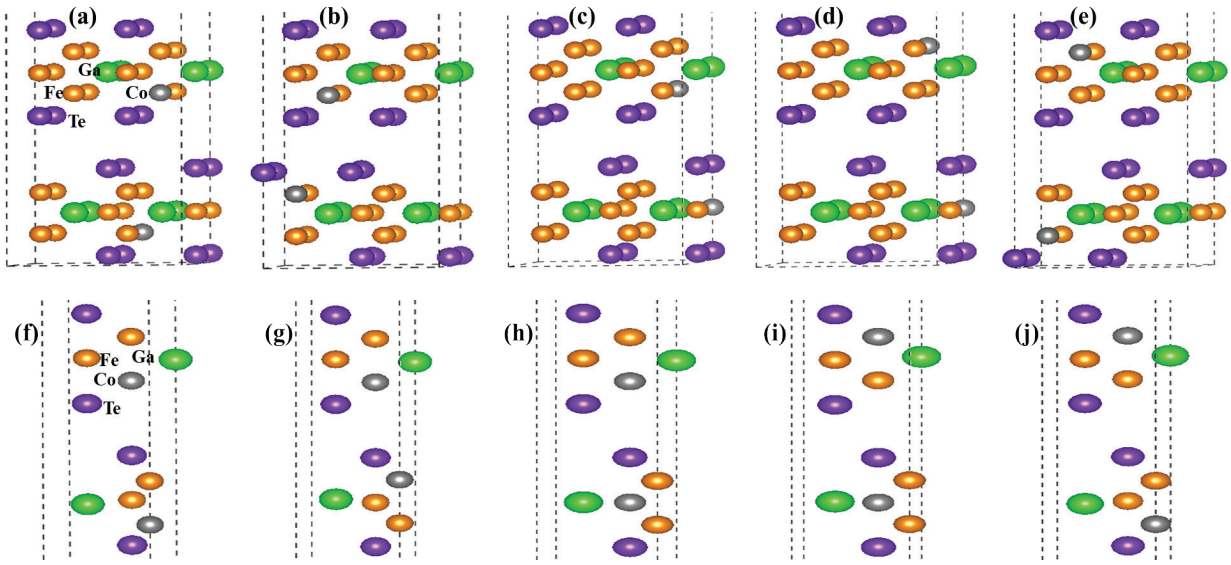

Fig. S1 Different random site Co doping in bilayer $Fe_{3-x}Co_xGaTe_2$ for **(a–e)** x = 0.083 and **(f–j)** x = 0.167.

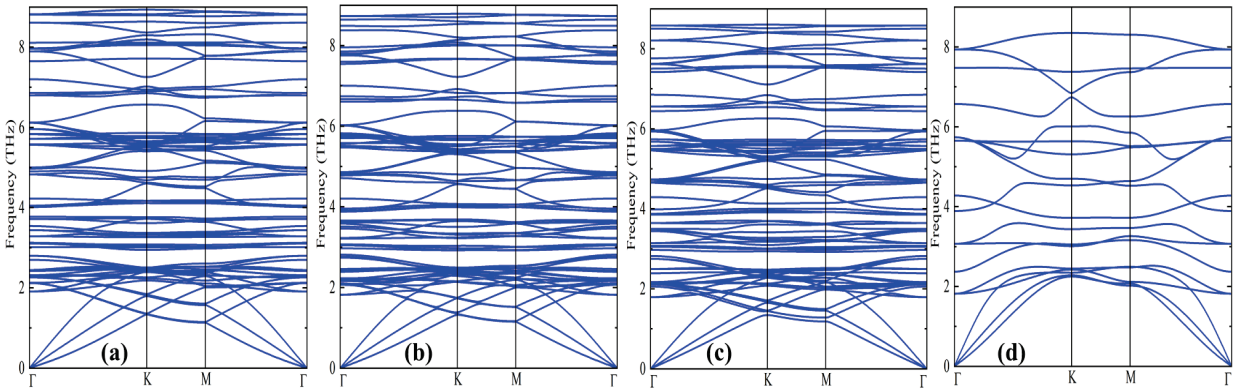

Fig. S2 Phonon band structure for Co doping in monolayer $Fe_{3-x}Co_xGaTe_2$ for **(a)** x = 0.083, **(b)** x = 0.167, **(c)** x = 0.25, and **(d)** x = 0.33.

Table S2 Average local magnetic moment (in μ_B/atom) of Fe, Co, Te, and Ga atoms in bilayer $Fe_{3-x}Co_xGaTe_2$ (x = 0.083, 0.167, and 0.250) systems.

Systems/Magnetic moments	**Fe_{center} (layer 1)**	**$Fe_{top(bottom)}$ (layer 1)**	**Fe_{center} (layer 2)**	**$Fe_{top(bottom)}$ (layer 2)**	**Co (layer 1)**	**Co (layer 2)**	**Te (Ga)**
$Fe_{2.917}Co_{0.083}GaTe_2$	1.51	2.41	1.48	2.40	0.85	0.84	-0.07 (-0.08)
$Fe_{2.833}Co_{0.167}GaTe_2$	1.57	2.57	1.54	2.46	0.86	0.85	-0.05 (-0.08)
$Fe_{2.75}Co_{0.25}GaTe_2$	1.64	2.52	1.62	2.52	0.88	0.87	-0.03 (-0.08)
$Fe_{2.67}Co_{0.33}GaTe_2$	---	2.57	---	2.58	0.91	0.93	-0.02 (-0.08)

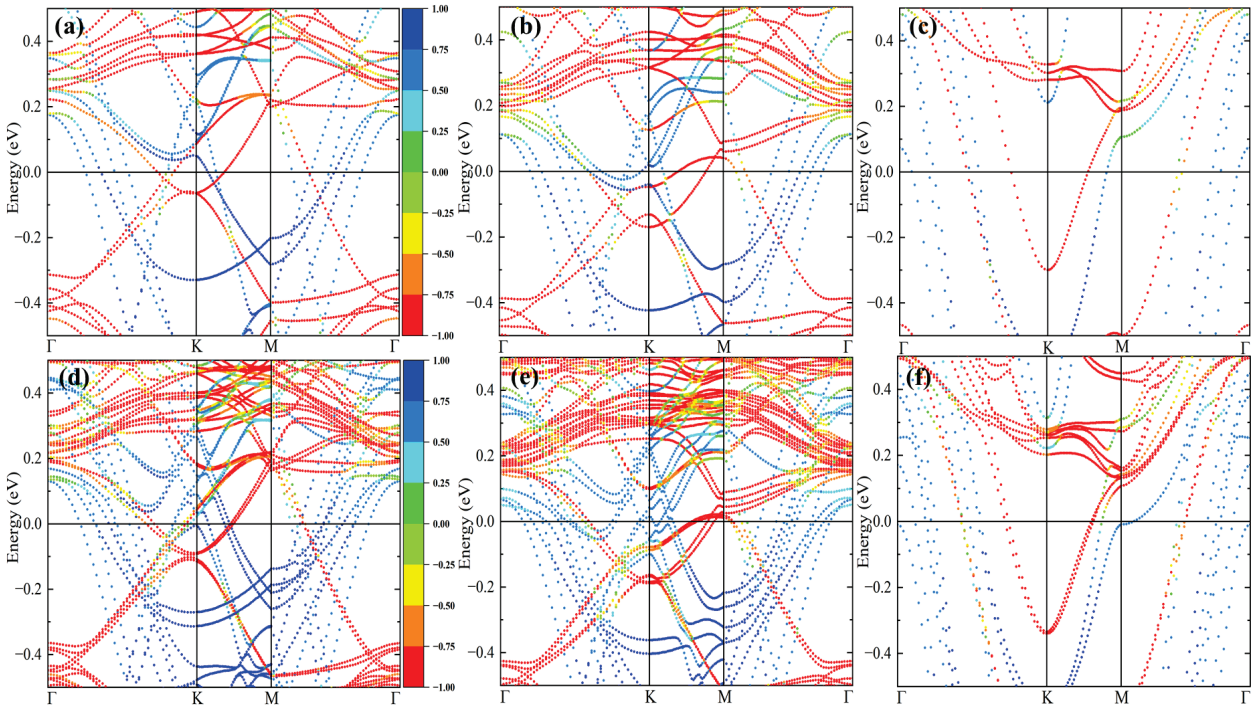

Fig. S3 Spin projected band structures including SOC for **(a)** monolayer $Fe_{2.833}Co_{0.167}GaTe_2$, **(b)** monolayer $Fe_{2.75}Co_{0.25}GaTe_2$, **(c)** monolayer $Fe_{2.67}Co_{0.33}GaTe_2$, **(d)** bilayer $Fe_{2.833}Co_{0.167}GaTe_2$, **(e)** bilayer $Fe_{2.75}Co_{0.25}GaTe_2$, and **(f)** bilayer $Fe_{2.67}Co_{0.33}GaTe_2$.

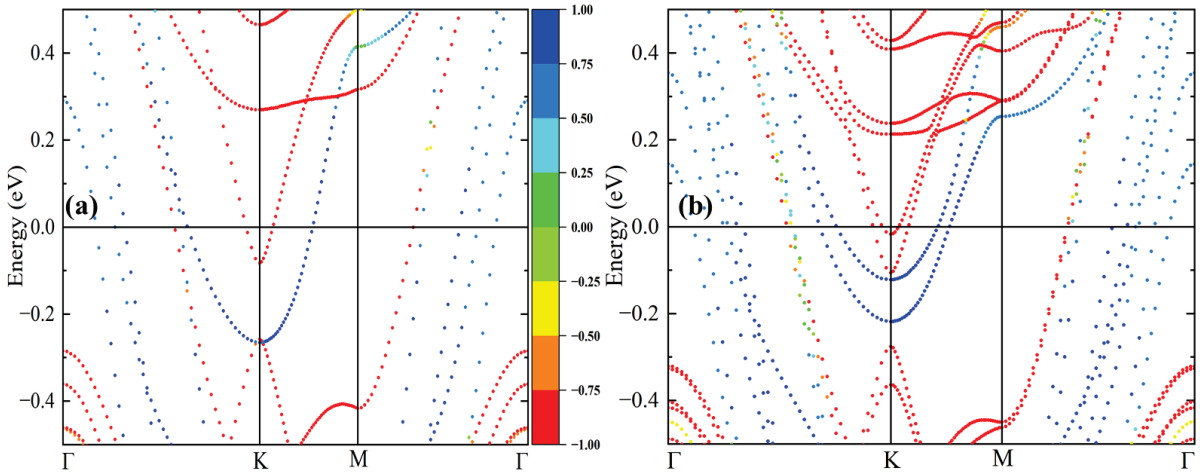

Fig. S4 Spin projected band structures including SOC for **(a)** monolayer Fe_3GaTe_2 and **(b)** bilayer Fe_3GaTe_2.

For comparison we also presents the spin projected band structures including SOC in monolayer and bilayer Fe_3GaTe_2 in Fig. S4 in SI. The band structures drastically changes after Co doping.

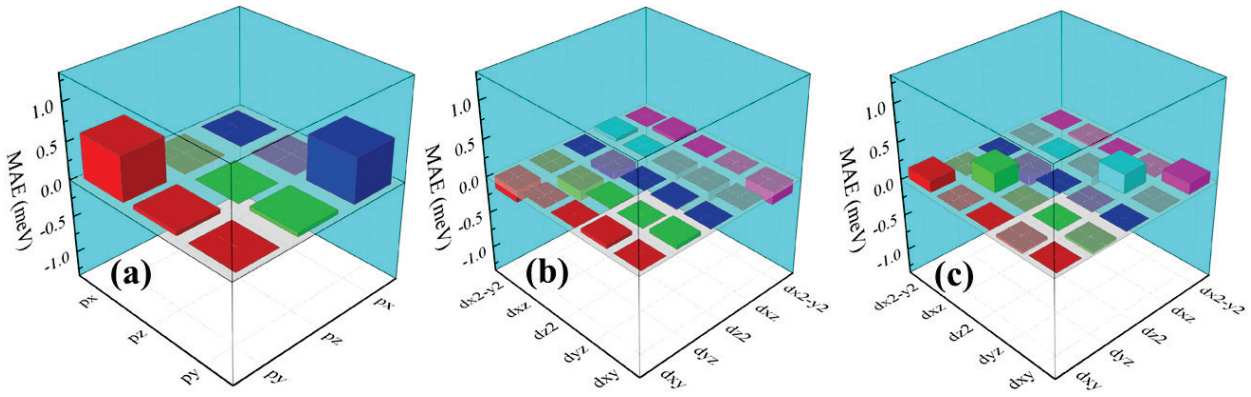

Fig. S5 SOC matrix analysis of monolayer Fe_3GaTe_2 **(a)** Te atom, **(b)** Fe-top atom, **(c)** Fe-center atom.

Figures S5(a)–(c) in the SI illustrates the SOC matrix elements of the Te, Fe-top, and Fe-center atoms in monolayer pristine Fe_3GaTe_2. Here the positive and negative values correspond to contributions to the out-of-plane and in-plane MAE. The main contribution to the MAE arises from the SOC in the (px-py) orbitals of the Te atoms as shown in Fig. S5(a). The Fe atoms in the top and bottom layer produce a small inplane MAE from the SOC in ($d_{x^2-y^2} - d_{xy}$) orbitals as shown in Fig. S5(b). The Fe atom in the central layer on the other hand produced small out-of-plane MAE from SOC in ($d_{x^2-y^2} - d_{xy}$) orbitals and (d_{xz}-d_{yz}) orbitals as shown in Fig. S5(c). Note that no substantial contribution to the magnetic anisotropy is found from Ga atoms in all the studied systems.

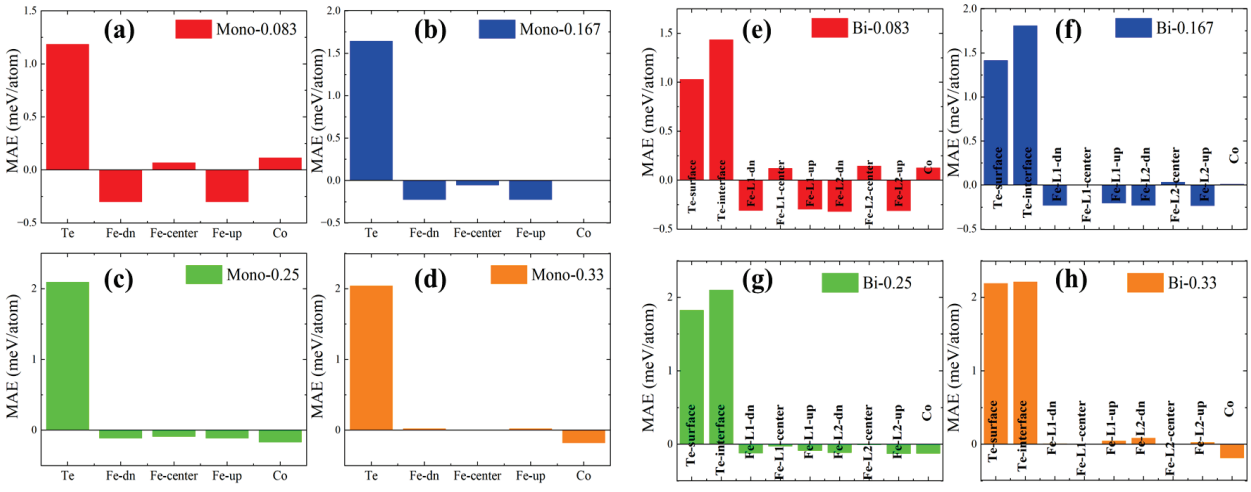

Fig. S6 Contribution to the total MAE of every system from Fe, Te, and Co atoms in different layers in monolayer and bilayer $Fe_{3-x}Co_xGaTe_2$ (x=0.083, 0.167, 0.25, and 0.33) systems.

For an overall comparison, we plotted the contribution to the total MAE of every system from Fe, Te, and Co atoms in different layers in monolayer and bilayer $Fe_{3-x}Co_xGaTe_2$ (x = 0.083, 0.167, 0.250, and 0.330) systems in SI Fig. S6. In monolayer $Fe_{3-x}Co_xGaTe_2$ (x = 0.083, 0.167, 0.250, and 0.330) systems (Figs. S6(a)–(d)), we can see that the main contribution originates from the Te atom and with an increase in Co doping it has an increasing trend. Besides, the Fe atoms in the top and bottom layer layers originate small in-plane contributions in all systems. Furthermore, the Fe atoms in the central layer and Co atoms originate very small out-of-plane contributions at x=0.083, but with higher Co doping it switches to a small in-plane contribution. In bilayer $Fe_{3-x}Co_xGaTe_2$ (x = 0.083, 0.167, 0.250, and 0.330) systems (Figs. S6(e)–(h)), once again the main contribution originates from Te atoms, however, the interface Te atoms are more sensitive compared to the surface Te atoms. The Fe atoms in the top, bottom, and central sublayers of both layers and Co atoms have similar behavior to that in monolayer $Fe_{3-x}Co_xGaTe_2$ (x = 0.083, 0.167, 0.250, and 0.330) systems.

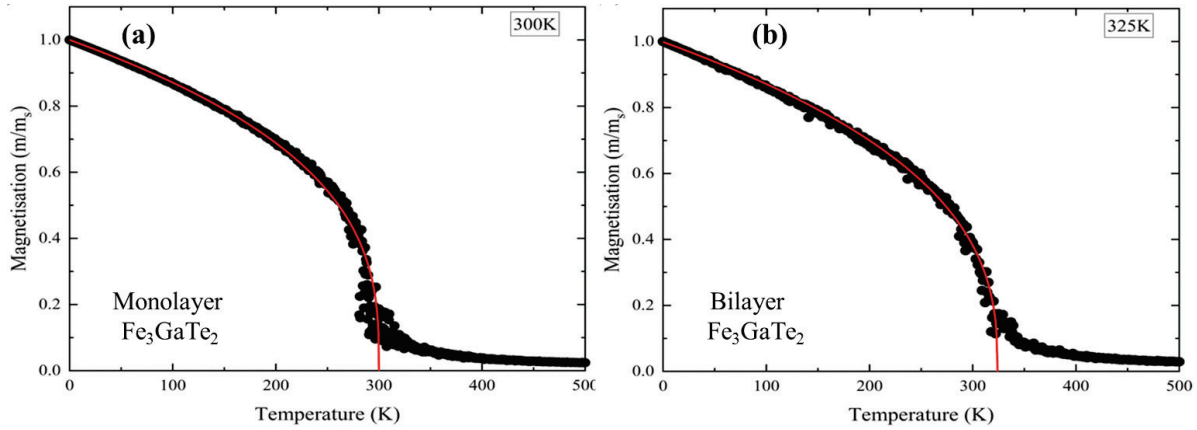

Fig. S7 Temperature-dependent magnetization curves in pristine **(a)** monolayer and **(b)** bilayer Fe_3GaTe_2 systems.

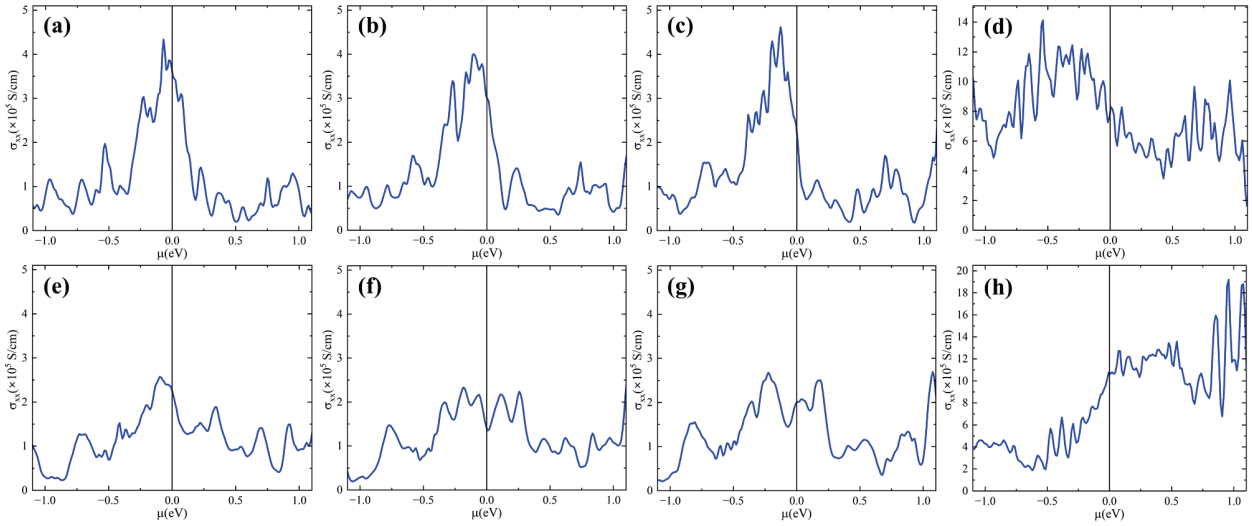

Fig. S8 Thickness-dependent longitudinal conductivity σ_{xx} for **(a)** monolayer $Fe_{2.917}Co_{0.083}GaTe_2$, **(b)** monolayer $Fe_{2.833}Co_{0.167}GaTe_2$, **(c)** monolayer $Fe_{2.75}Co_{0.25}GaTe_2$, **(d)** monolayer $Fe_{2.67}Co_{0.33}GaTe_2$, **(e)** bilayer $Fe_{2.917}Co_{0.083}GaTe_2$, **(f)** bilayer $Fe_{2.833}Co_{0.167}GaTe_2$, **(g)** bilayer $Fe_{2.75}Co_{0.25}GaTe_2$, and **(h)** bilayer $Fe_{2.67}Co_{0.33}GaTe_2$ systems.

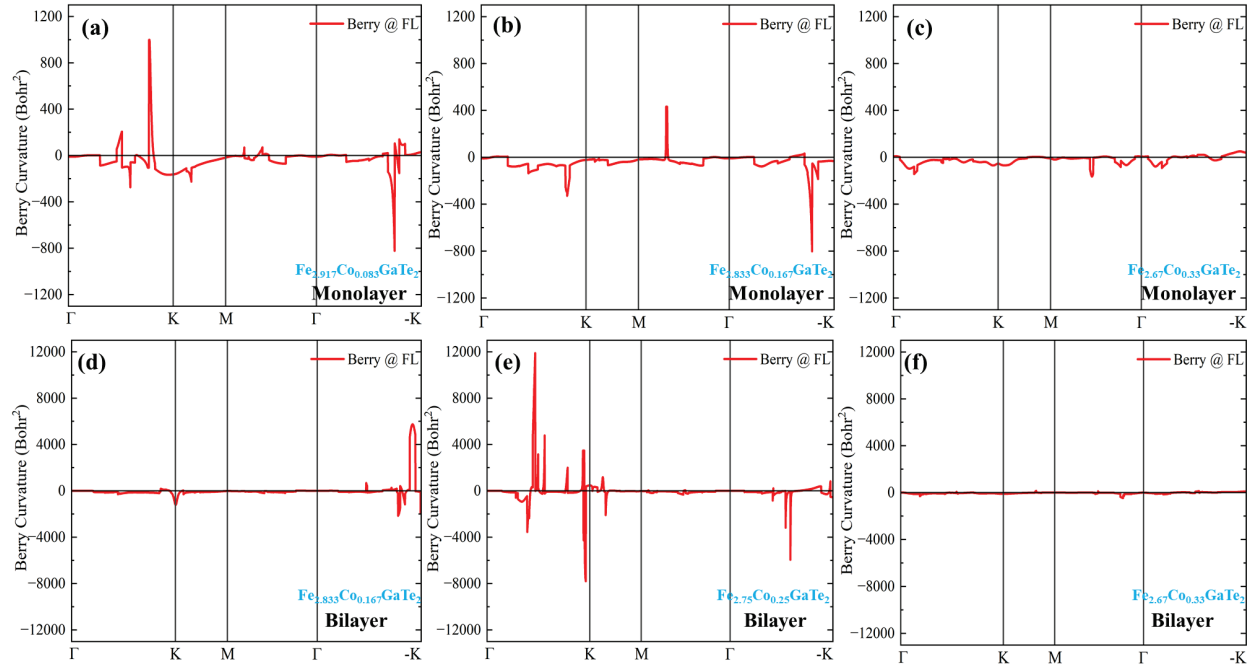

Fig. S9 Berry curvature along high symmetry lines for **(a)** monolayer $Fe_{2.917}Co_{0.083}GaTe_2$, **(b)** monolayer $Fe_{2.833}Co_{0.167}GaTe_2$, **(c)** monolayer $Fe_{2.67}Co_{0.33}GaTe_2$, **(d)** bilayer $Fe_{2.833}Co_{0.167}GaTe_2$, **(e)** bilayer $Fe_{2.75}Co_{0.25}GaTe_2$, and **(f)** bilayer $Fe_{2.67}Co_{0.33}GaTe_2$.